MISSION ANALYSIS FOR PICO-SCALE SATELLITE BASED DUST DETECTION IN LOW EARTH ORBITS

by

JACOB BELLI
B.S. Mississippi State University, 2011

A dissertation submitted in partial fulfillment of the requirements
for the degree of Master of Science
in the Department of Mechanical and Aerospace Engineering
in the College of Engineering and Computer Science
at the University of Central Florida
Orlando, Florida

Summer Term
2013

Major Professor: Yunjun Xu

ABSTRACT

A conceptual dust detection mission, KnightSat III, using pico-scale satellites is analyzed. The purpose of the proposed KnightSat III mission is to aid in the determination of the size, mass, distribution, and number of dust particles in low earth orbits through a low cost and flexible satellite or a formation of satellites equipped with a new dust detector. The analysis of a single satellite mission with an on-board dust detector is described; though this analysis can easily be extended to a formation of pico-scale satellites. Many design aspects of the mission are discussed, including orbit analysis, power management, attitude determination and control, and mass and power budgets. Two of them are emphasized. The first is a new attitude guidance and control method, and the second is the online optimal power scheduling. It is expected that the measurements obtained from this possible future mission will provide insight into the dynamical processes of inner solar system dust, as well as aid in designing proper micro-meteoroid impact mitigation strategies for future man-made spacecraft.

I want to dedicate this thesis to my parents, Keith and Monique Belli. Their love and support throughout my upbringing has brought me to this point in my life and without them I would have never gotten this far. They always pushed me to do my best in school and told me if I did my best, there was nothing that I couldn't accomplish. So I can attribute my success in my schooling and my completion of this thesis directly to them. Thank you.

ACKNOWLEDGMENTS

First of all, I would like to thank my advisor, Dr. Yunjun Xu, for the support and direction he has given me throughout my Master's research. His willingness to give his time whenever I needed aid, in addition to the financial support he secured for me, has been very much appreciated.

I would also like to thank the rest of my committee, Dr. Kuo-Chi Lin and Dr. Todd Bradley, for their continued support in advancing my research. A special thanks also goes out to Dr. Richard Eastes and the Florida Space Institute, for providing financial support and opportunities for collaboration with experts in the aerospace field.

I would like to give a final thanks to my lab mates in the Control and Dynamics lab. Your assistance with sharing ideas, brainstorming, and general aid was invaluable.

TABLE OF CONTENTS

LIST OF FIGURES

LIST OF TABLES

CHAPTER ONE: INTRODUCTION

Due to the advancements in small satellite technologies, it is possible for pico-scale satellites to become a viable, low-cost alternative to larger satellites for the purpose of conducting meaningful scientific missions. They can be designed to fit within a one-to-six unit (1U to 6U) specification, with each unit being constrained to a 10x10x10 cm^3 volume and 1.3 kg mass[1]. These units can then be launched within a single standardized container known as the P-Pod[1,2].

To enhance the mission capability, multiple pico-scale satellites can be grouped in a formation to replace a single large satellite. The benefits of the formation flying system include the ability to reconfigure while in orbit to expand the amount of missions possible, and the ability to add, replace, or upgrade existing satellites in orbit without losing mission capabilities[3]. Additionally, a formation of pico-scale satellites offers lower manufacturing cost due to mass production techniques, minimal financial loss in case of failure, and a reduced size and complexity of the individual satellites. Finally, a formation of pico-scale satellites can accomplish the same missions as a larger satellite even though, for certain missions, it is necessary to have multiple pico-scale satellites working cooperatively in order to achieve the same observation performance as that of a single large satellite[3].

From a scientific point of view, there are several key reasons to study the dust environment around a planet. For example, the Moon does not have a significant atmosphere to prevent micrometeorites from hitting the surface. Micrometeorite bombardment of the surface affects the regolith composition and morphology and also ejects neutral atoms that contribute to

the exosphere of the Moon[4]. Mercury is subject to the same process, and although much further away than the Earth-Moon system, models for the micrometeorite impacts at Mercury are based on extrapolations from measurements of this population at Earth[5]. Another example is that constraining the abundance of dust in Earth orbits helps to constrain models of the origin of these populations and provides insight into inner solar system dynamical processes. An additional benefit to flying dust detectors in a low earth orbit is to aid in the proper design of micro-meteoroid impact mitigation strategies for future man-made spacecraft.

Our mission, based on a pico-scale satellite called KnightSat III, has several anticipated benefits associated with it. The first, as mentioned previously, is that the data generated can give valuable information concerning the distribution and size of dust in near earth orbits. This distribution can be used to design dust impact mitigation systems for future satellites. Additionally, the power management scheduler that has been created can improve the self-sufficiency of satellites in orbit. Since the satellite is not in constant communication with the ground, a procedure that can allow the satellite to continue operations after an unforeseen circumstance would be useful on any satellite, not just small satellites.

The proposed contributions of this research are as follows: (1) An in depth look at the feasibility of a dust detection mission on a pico-scale satellite, (2) the design of an online power management system that has not been given much attention in satellite mission literatures, and (3) a new online attitude guidance and control method that can rapidly generate fuel efficient attitude trajectory.

This research work will be broken up into three major sections. The first section deals with the description of the payload and the orbit analysis. It will cover general orbit information

along with the specifics of the dust detector. The second section will detail information about the design of the individual subsystems of the satellite bus. Our new attitude control method will be discussed here as well. The third and final section will describe the power management strategy that will be implemented in the satellite. The specific subsystem models will be discussed, as well as the cost function and a set of preliminary results.

CHAPTER TWO: MISSION ANALYSIS

The goal of this mission is the use of the dust detector to determine the size, mass, distribution, and number of dust particles in low earth orbits. In order to accomplish this mission, a dust detector is designed based on previous dust detectors, and a proper orbit is chosen that will best fit the objectives and restrictions of the dust detection mission. The analysis of a single dust detection satellite is described; though this analysis can easily be extended to a formation of pico-scale satellites as well.

Scientific Payload – Dust Detector

The design of the dust instrument is driven by the science objectives as well as the goal of placing the instrument on a single KnightSat III or a distributed system of KnightSat IIIs. The major components of the instrument are the detector, detector electronics, transmitter and receiver, and a power system. The design is based on previous small dust detectors built by others[6,7]. The detector will consist of a permanently polarized polyvinylidene fluoride (PVDF) thin film. Detector electronics will consist of an Amptek 225 charge sensitive amplifier (CSA) with lead wires attached to the edge of the detector. A CSA is an amplifier with high input impedance that converts charge pulses into voltage pulses that are then passed to other amplifiers in the chain. The detector will be mounted to a fiberglass back (non-conductive circuit board), which will be mounted to the exterior of one side of the satellite. Tests of PVDF dust detectors where the PVDF material is suspended in a frame show that the PVDF is subject to vibrations,

which is a significant source of noise. The fiberglass backing will minimize vibrations thereby decreasing noise. A schematic of the proposed dust detector is shown in Figure 1.

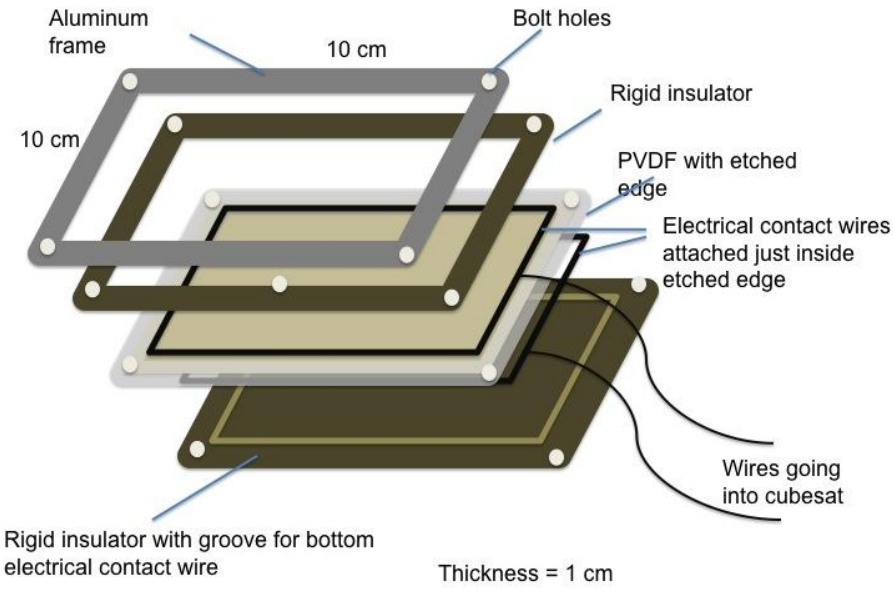

Figure 1: Schematic of Dust Detector

When a dust particle above the detection threshold hits the PVDF thin film, a charge of electrons is produced. The number of electrons produced is given by[8]

$$N_e = 3.8 \times 10^{17} m^{1.3} v^3 \qquad (1)$$

where m is the impacting particle's mass in grams and v is the impact velocity in km/s. The CSA has a shaper output whose height is proportional the number of charges at the input of the CSA and therefore is proportional to the velocity and mass of the impactor. For testing purposes, the output of the CSA is connected to a digital oscilloscope in trigger mode that captures the

short duration signal. For flight, the output of the CSA will be connected to a peak hold circuit with a decay time of a few milliseconds in order to extend the time of the pulse. The output of the peak hold circuit is connected to an ADC that records a digital signal proportional to the amplitude of the pulse.

The Cosmic Dust Experiment[7] (CDE) consisted of 12 sensor patches that were 14.2 X 6.5 cm^2 each, providing a total surface area of ~ 0.1 m^2, whereas a single dust detector proposed here is 10 X 10 cm^2 (0.01 m^2). Using published data[7] for impact rates encountered with the CDE and scaling to the size of our detector, we estimate 1 impact every 1-2 weeks for grains with mass from $10^{-12}<m<10^{-9}$. Since we plan to mount two dust detectors on a 3U KnightSat III with an area of 0.04 m^2, we expect 4 impacts every 1-2 weeks.

One major drawback of the dust detector design is that extreme fluctuations in temperature can cause significant amounts of noise to be generated[7]. This noise comes from flexure in the structure of the satellite caused by rapid heating or cooling from the craft entering or leaving an eclipse. The flexure in the structure causes a similar flexure in the PVDF material, which leads to false signals being generated. These concerns are well documented and will have a significant effect on the desired orbit.

Orbit Analysis

The satellite's orbit will have a significant impact on the amount of thermal cycling the craft will experience. As such, a circular, sun-synchronous orbit was chosen with the main goal of significantly reducing the eclipse times experienced by KnightSat III. The orbital elements are shown in Table 1.

Table 1: Orbital Elements of the Proposed KnightSat III Mission

Altitude	Eccentricity	Inclination	Right Ascension	Argument of Perigee
750 km	0	98.4 deg	0 deg	N/A

There are several benefits associated with choosing a sun-synchronous orbit for this mission. (1) As stated previously, a sun-synchronous orbit will mitigate the thermal cycling issue during a majority of the orbit, as the craft will stay illuminated by the sun throughout the most of its orbit. (2) The extended illumination time of the solar panels allows for a larger power budget due to the increased amount of power generated throughout the course of an orbit. This produces a larger amount of flexibility in the system as power concerns are generally not an issue as long as the craft stays illuminated. (3) A long period of sunlight exposure also minimizes the number of batteries that would normally be needed to power the craft during eclipses. This saves space within the interior of the craft as well as reduces the mass budget. Due to the limited space within a pico-scale satellite, significant station-keeping maneuvers cannot be performed. As a result, the initial sun-synchronous orbit will immediately begin to experience small perturbations from solar radiation pressure, the J_2 effect, etc., leading to a gradual orbital decay. While the effects do not have a large effect on any of the major orbital parameters within the mission lifetime, the perturbations are significant enough to cause the pico-scale satellite to deviate from the precise orbit that will naturally regress in time with the revolutions of the Earth. This leads to an approximate four-month period of time when KnightSat III will experience eclipses of gradually increasing duration. These eclipses are initially very small, starting at roughly 0.15 minutes in length. As time passes, they will gradually increase until they reach a maximum of 20

minutes at the midpoint of the eclipse period (about 2 months in). Once the midpoint is passed, the eclipses will decrease in duration, until the craft returns to a permanent illuminated state. This eclipse period occurs after the first four months that the satellite is in orbit.

Since the satellite will experience some eclipses, the thermal cycling must once again be addressed during this period. A thermal strategy is developed to help mitigate the thermal cycling issue, and will be discussed in a later section.

CHAPTER THREE: SUBSYSTEM DESIGN

An equally important part of the mission design is the design of the satellite bus. The subsystems within the bus support the mission by keeping the satellite functional. These designs are detailed in the following sections.

Structure

The structure of the satellite is designed based on the external requirements placed on it by the CubeSat launch interface[2]. An isogrid structure machined from Aluminum 6061 was chosen to save weight. Additionally, the moments of inertia of the off-diagonal components are very small. The frame was designed to resist up to a 7.7g maximum axial launch load based on the qualification requirements[1]. A CAD drawing of the design is shown below in Figure 2, along with a fabricated prototype structure.

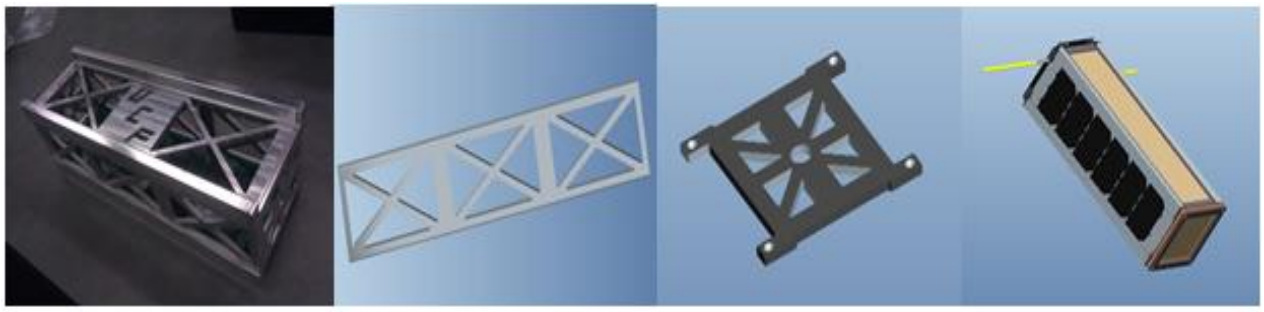

Figure 2: Fabricated Prototype, Side Panel, End Panel, Full Satellite with Solar Panel

After performing a load analysis on the structure using SolidWorks, it is found that the maximum stress experienced by the structure with the 7.7g axial load applied is only 250 kPa

and the maximum strain on the structure is 2.8 με. Additionally, the structure is found to be displaced by a maximum of 7.4×10^{-4} mm. These analyses, shown in Figure 3, indicate that our structural design satisfies the launch load requirements.

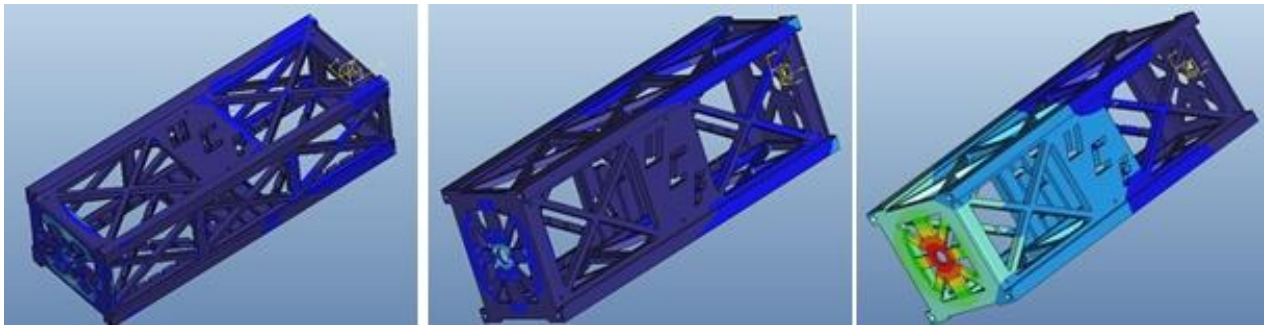

Figure 3: SolidWorks Stress, Strain, and Displacement Models

Command and Data Handling (C&DH)

Our C&DH unit is chosen to be the Cube Computer[9] produced by the Electronic Systems Laboratory (ESL). This computer is a high performance, lightweight, and low power (< 1.5W) product that is suitable for C&DH, Telemetry, Tracking & Command (TT&C), data archival, and attitude determination and control (ADC). The microcontroller for this board is a 32-bit ARM Cortex-M3 based MCU. It has 256 kB of EEPROM, 4 MB of flash memory, eight 12-bit A/Ds, two external SRAM with 1 MB of storage, and a socket for up to a 2 GB MicroSD card. The 4 MB of onboard flash memory will be the main data storage medium for the C&DH operating system, with the MicroSD card serving as the storage for telemetry, payload data, and any additional code. Payload and telemetry data will be temporarily stored on the external SRAM before transmission to prevent data loss due to corruption. Data will be stored for two weeks

before being cleared to make room for new data. The power consumption for each process of the CPU is shown below in Table 2.

Table 2: Cube Computer Process Power Consumptions

Mode	Power (mW)	Mode	Power (mW)
Mathematical Calculations	170	Stop/Sleep Mode	135/130
MicroSD storage/retrieval	435/310	UART Serial Communication	230
Analog-to-Digital Converter	150	SRAM (on-board memory storage)	155

Additionally, the computer's mass is only 65.84 grams, with the proper dimensions to fit easily into our structure. As it is compatible with the Cubesat Standard and with other products from many cubesat subsystem manufactures (e.g. ISIS, ClydeSpace, etc.), it has a high ease of integration with our other hardware.

Communications

The transceiver chosen is the ISIS TRXUV VHF downlink/UHF uplink Full Duplex Transceiver[10]. It has a downlink data rate of up to 9,600 bps, an uplink data rate of 1,200 bps, and a mass of 85 grams. The transmitter frequency range is a single frequency in a 130-160 MHz range, and the receiver frequency range is 400-450 MHz, both of which are compatible with amateur radio bands. The transmission frequency will be chosen from several amateur radio bands, as a license is easily obtainable. The expected power requirement for the transceiver is 0.2W when only the receiver is active and 1.7W for transmission. The receiver must always be active due to the International Telecommunication Convention's radio regulation 22.1 which

states that space stations must be fitted with a device that can immediately terminate any radio emissions from the craft by a telecomm and whenever required[11]. As a result, the minimum power requirement for the transceiver is 0.2W. This transceiver model has flight heritage beginning in 2012 onboard the PWSAT[10].

The chosen antenna is the ISIS Turnstile Configuration Deployable Antenna System for Cubesats[12]. It has a nominal power of less than 20 mW and a maximum power of 2W during deployment. It also has a maximum RF power requirement of 2W. This antenna is designed for combination with our specific transceiver, and has a mass of less than 100 grams. This particular antenna model also has flight heritage, and has been operational since July of 2010 onboard StudSat[12].

Taking the maximum upper power limit along with the minimum lower limit gives a total power range of 20 mW to 2 W. However, due to the requirement that the receiver always be active, the minimum standby power will be the combination of the 20 mW and the 0.2W minimums. This yields a total minimum power limit of 0.22W. Additionally, the communication subsystem will have a total mass of 185 grams.

The data produced by the dust detector is well within the range of data that can be downlinked to the ground during any given access window. A typical data package to be downlinked to the ground station includes two parts; payload data and telemetry data. The telemetry data will be downlinked whenever ground access is available, and the payload data will only be downlinked whenever it is obtained from the dust detector. Sets of data estimates are shown below in Tables 3 and 4.

Table 3: Payload Data Package

Package ID	Dust Strike Data	Time	Attitude	Temp.	Checksum	Total
8 bits	16 bits	32 bits	128 bits	12 bits	16 bits	212 bits

Table 4: Telemetry Data Package

Package ID	Time	Attitude	Angular Rates	Battery Level	Temp.	Checksum	Total
8 bits	32 bits	128 bits	96 bits	8 bits	12 bits	16 bits	300 bits

The four attitude quaternions and three angular rates are floating-point decimal values with 32 bit precision, and typically time values are stored as a 32 bit integer representing the number of seconds elapsed from a certain reference date and time. The package identifier indicates the start of the transmission and identifies the set of data to follow. The checksum is mathematically related to all of the data that precedes it in such a way that it can be used to verify the integrity of the received data. The other values are based on the expected precision necessary to get an accurate description of the subsystem performance. As can be seen from the table, the total download size of the combined packages is only 512 bits which is well below the available downlink data rate.

Thermal

The thermal design of the satellite is highly dependent on the special requirements of the dust detector. In order to mitigate the thermal cycling of the satellite, a proper heater must be chosen, not just for the operation of internal components, but also in an attempt to regulate the temperature of the satellite structure itself.

The external temperature was modeled using the typical spherical model for satellites. The temperature of the worst case scenarios are calculated using the following equations[13],

$$T_{max} = \left[\frac{0.25 P_{solar} \alpha_s + q_{IR} \varepsilon_{IR} F_{s\_e} + P_{solar} a_e \alpha_s K_a F_{s\_e} + \frac{Q_w}{\pi D^2}}{\sigma \varepsilon_{IR}} \right]^{0.25} \quad (2)$$

$$T_{min} = \left[\frac{q_{IR} \varepsilon_{IR} F_{s\_e} + \frac{Q_w}{\pi D^2}}{\sigma \varepsilon_{IR}} \right]^{0.25} \quad (3)$$

$$F_{s\_e} = 0.5 \left(1 - \frac{\left(H^2 + 2HR_E \right)^{0.5}}{H + R_E} \right) \quad (4)$$

where P_{solar} is the solar constant in W/m^2, α_s is the solar absorptivity of anodized black paint, q_{IR} is the Earth's infrared emission, ε_{IR} is the infrared emissivity of anodized black paint, F_{s_e} is the view factor from the sphere to the earth, a_e is the albedo of the Earth, K_a is a factor that accounts for the reflection of collimated incoming solar energy off a spherical Earth, Q_w is the electrical power dissipation of the internal components in watts, D is the diameter of the spherical spacecraft in meters, σ is the Stefan-Boltzmann constant, H is the altitude of the spacecraft in km, and R_E is the radius of the Earth in km.

As the satellite is not a sphere, the spherical diameter is an approximation found by taking the actual surface area of the satellite and finding the diameter of a sphere with an equivalent surface area[13]. Using the previous values, a temperature range of 43° to -65°C is found. The craft will experience the full range of values over its lifetime, although the temperature will stay fairly constant during the long periods of full exposure to the sun without eclipses, as shown in Figure 4.

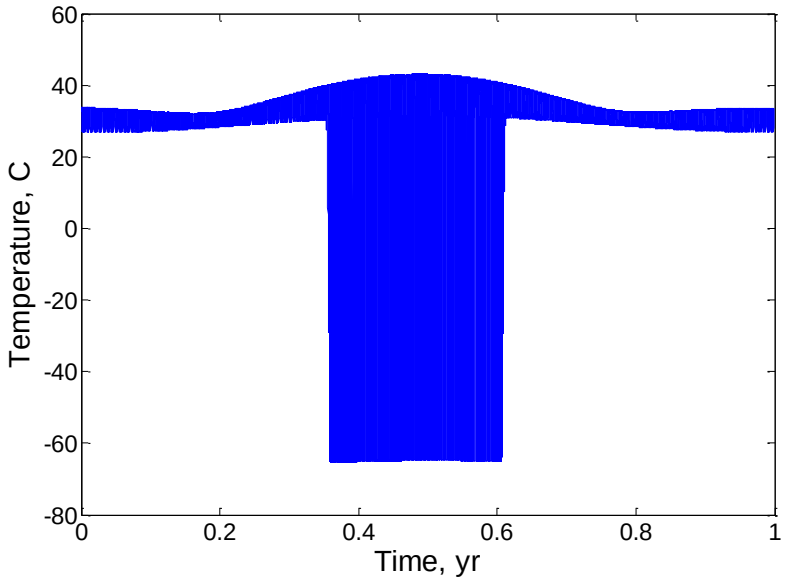

Figure 4: Thermal Cycle over One Year

Based on this analysis, the satellite will only need active thermal management during the four-month period of eclipses, since the passive thermal strategy of the properly chosen outer coating keeps the satellite within a narrow range of temperatures during its time in full sunlight, which will mitigate any thermal cycling issues. However, as this is only a very rough calculation, a more in depth thermal analysis was performed on a CAD model of our satellite. A model of the

satellite structure, solar panel, and simplified models of the internal components including; batteries, CPU chip, power converter chip, transceiver, and ADCS were created and assembled in Solidworks. A low density mesh was used in order to reduce simulation run times. The three circuit boards and the ADCS were designated as heat generation sources. The external structure radiates heat to the ambient temperature of space (4 Kelvin). The internal components radiate heat to the ends of the satellite, and the circuit boards radiate heat to each other. Additionally, five small, flexible heaters were placed at central points on the structure in order to attempt to stabilize the structural temperature and keep it relatively warm compared to the estimated 43°C daytime temperature

The study is a steady state, cold case scenario. All of the internal components are modeled as running at minimal power. The satellite is also assumed to be in eclipse. This scenario gives the worst case situation for the temperature of the satellite, which will also be the time when the structure would experience the most flexing due to the rapid cooling as it entered eclipse. The heaters are assumed to output 0.4W of power each, which is the maximum amount of power we have allocated to the thermal subsystem. As is shown in Figure 5, the outer structure's approximate temperature varies from -10°C to 21°C.

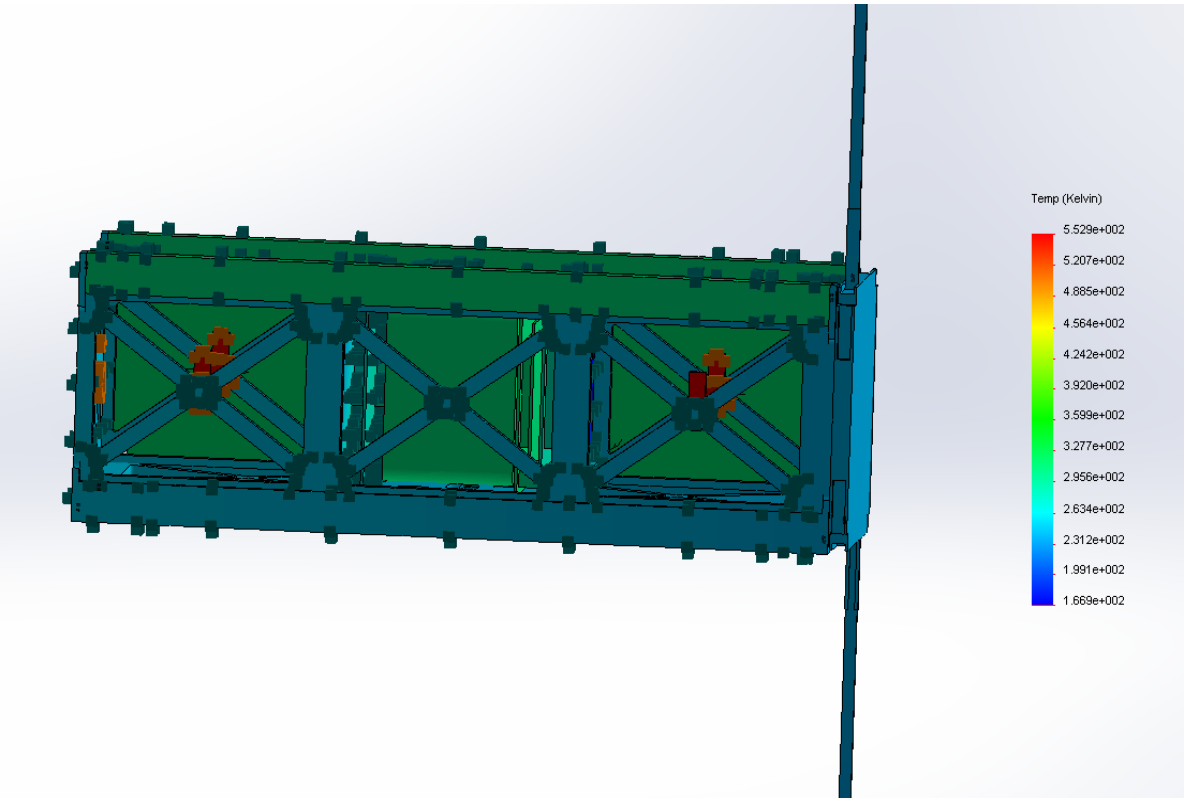

Figure 5: Cold Case Thermal Analysis

This scenario implies that there is enough heat generated by placing small heaters on the structure to help mitigate the extreme temperature swings that accompany the satellite's transition into eclipse. The predicted temperature of -65°C was raised to an average temperature of 5.5°C, which will be warm enough to help prevent the structural flexing. Additionally, while the temperature is much less than the hot case temperature of 43°C, it is also represents a gradual cooling over a 20 minute period, rather than a sudden drop to -65°C within a few minutes of entering eclipse. This should also help to diminish any structural flexing that would accompany a more rapid cooling. The placement and final power requirements of the heaters will be

determined during hardware testing of the satellite. For now, 250 grams and 2 Watts have been allocated to the mass and power budgets respectively.

ADCS

The attitude of KnightSat III will be determined by the 3-axis magnetometer and sun sensors inside of the complete MAI-100 ADCS[14], which has a pointing accuracy of 1° and a maximum torque of 0.635 mN x m. Two recently developed algorithms will be applied to the attitude guidance and control system. First, the attitude slewing and spinning guidance commands will be generated through a new real-time nonlinear constrained optimal control method[15]. Second, a nonlinear robust adaptive control method will be used to track the generated optimal guidance command of the first algorithm[16]. Both algorithms have been simulated in MATLAB, and verified in a ground-based testbed. Our 1-U and 3-U testbeds are shown below in Figures 6 and 7.

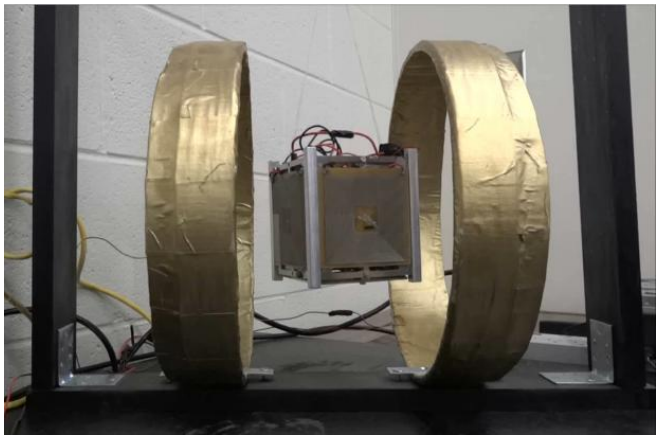

Figure 6: 1-U Ground Testbed

Figure 7: 3-U Ground Testbed

First, a varying manifold based, nonlinear constrained optimal trajectory planning method is used for the large attitude slewing and spinning maneuvers' guidance command generation[15]. The performance index to be minimized is the power consumption of the attitude control system, and the constraints may include the current to the ADCS $(I_{\min}, I_{\max})$, and the angular velocity $\|\omega_B\| \le \omega_{\max}$. The optimal guidance commands will minimize the power usage, while providing three-axis attitude guidance and the desired pointing accuracy. The salient features of this varying manifold based method are: (1) it can significantly reduce the dimension of the achieved nonlinear programming problem (NLP), and (2) it can find the optimal solution rapidly considering state and control inequality and equality constraints. Figure 8 shows a single-axis,

ground-based demonstration of this algorithm with magnetic torqueing where the attitude quaternion q_2 corresponds to the vertical axis and $q_{2,desired} = 0.2$.

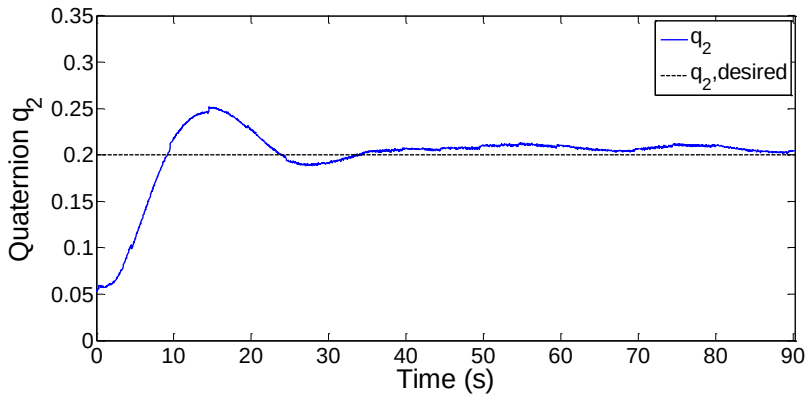

Figure 8: Varying Manifold Based Optimal Control Tested on the Ground Based Testbed

A recently developed adaptive controller will be adopted for precise pointing and attitude disturbance rejection[16]. Figure 9 shows an example of the performance achieved on the actual hardware testbed. The advantages of this control method are that: (i) the attitude can be quickly stabilized even with unknown high-frequency gain, unknown parameters (e.g. the moment of inertia), and bounded disturbances (e.g. the magnetic field), and (ii) a fast adaptation and satisfactory transient response can be guaranteed with stable tracking performance.

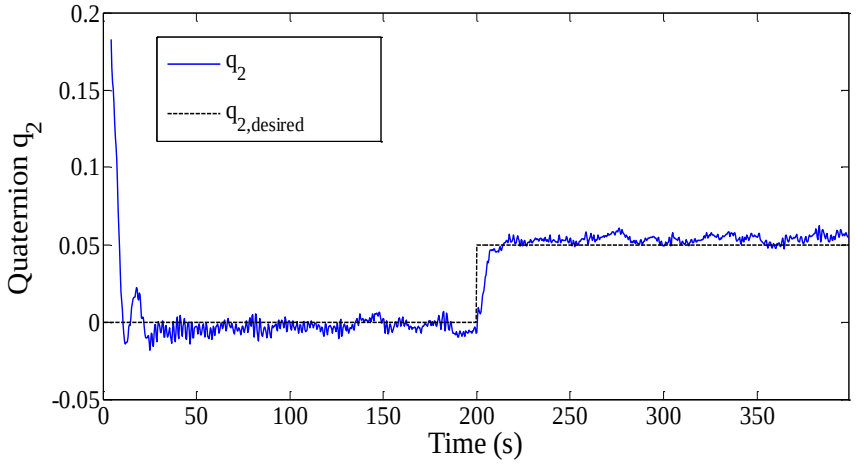

Figure 9: Robust Adaptive Control Results

Mass Budget

Table 5 shows the mass budget for the KnightSat III design. As stated previously, the maximum allowable mass for a 1-U pico-scale satellite is 1.3 kg. Since our satellite is a 3-U type, the maximum allowable mass is equivalent to 4 kg. As can be seen in the table, our satellite is well below the mass limit, even taking into account a 5%, 200 gram factor of safety. Since we are still in the conceptual design phase, a large mass margin is beneficial so there will be plenty of additional mass should unforeseen circumstances arise.

Table 5: Mass Budget of KnightSat III

Subsystem	Allocated Mass (grams)	Mass Estimate (grams)	Surplus/Deficit (grams)
Structure	1000	910	+90
Thermal	250	100	+150
ADCS	900	865	+35
C&DH	150	70	+80
Communications	250	185	+65

Subsystem	Allocated Mass (grams)	Mass Estimate (grams)	Surplus/Deficit (grams)
Power	950	895	+55
Payload	300	100	+200
Total Allocated	3800	3125	+675
System Contingency	200	200	
Total Mass	4000	3325	+675

Power Budget

The power subsystem consists of one panel of triple junction solar cells with 28.3% efficiency[17], and a set of Lithium polymer cell batteries[18]. The unregulated voltage provided by these systems is 8.2V to 14V, with a 5V regulated voltage and up to 355mA of current. The power budget over the course of one orbit is detailed in Table 6 below. Similar to the mass budget listed previously, there is a large amount extra power available in addition to the allocated margin. This can be explained through a number of reasons: (1) the uncertainty in the thermal subsystem leads to a much larger allocated margin that will be further refined in the future, (2) all of the subsystems will not necessarily be operating separately from each other, so there needs to be extra available power to handle concurrent power usage cases, and (3) the total power is based on the average power that is used by the system over an orbit, so should a subsystem actually be at peak power usage, it will severely cut into the power surplus. Thus, it is desirable to have the extra power available should it become needed.

Table 6: Power Budget of KnightSat III

Subsystem	Allocated Power (W)	Standby Power (W)	Peak Power (W)	On Time	Avg. Power (W)	Surplus/Deficit (W)
Thermal	2	0	2	20%	0.4	+1.6
ADCS	2	1.5	4.5	5%	1.65	+0.35
C&DH	0.725	0.13	1.14	30%	0.433	+0.292
Communications	0.4	0.22	2	5%	0.309	+0.091
Payload	0.5	0	1	1%	0.01	+0.49
Total Allocated	5.625	1.85	10.64		2.802	+2.823
System Contingency	0.625				0.625	
Total Power	6.25				3.427	+2.823

The standby and peak powers shown come from the hardware specifications and current best estimates. The average power is determined through a weighted average of the peak and standby powers using the projected active times as the weighting factor, and the variance is the difference between the allocated power and the average power expected. Since there is 6.25 W of power available instantaneously, the budget only needs to account for there being more power available on average over the course of the orbit, rather than always allocate a larger amount than the peak power. However, though there is sufficient power available for multiple systems to be active, there exists the possibility that more systems would request power than is possible to provide. It is these cases that the optimal power management strategy will be used to alleviate. In addition to the power budget shown above, a preliminary plot of the power usage versus power generation was created. This plot (shown in Figure 10) details a typical orbit, assuming that all the systems are active at some point within that particular orbit.

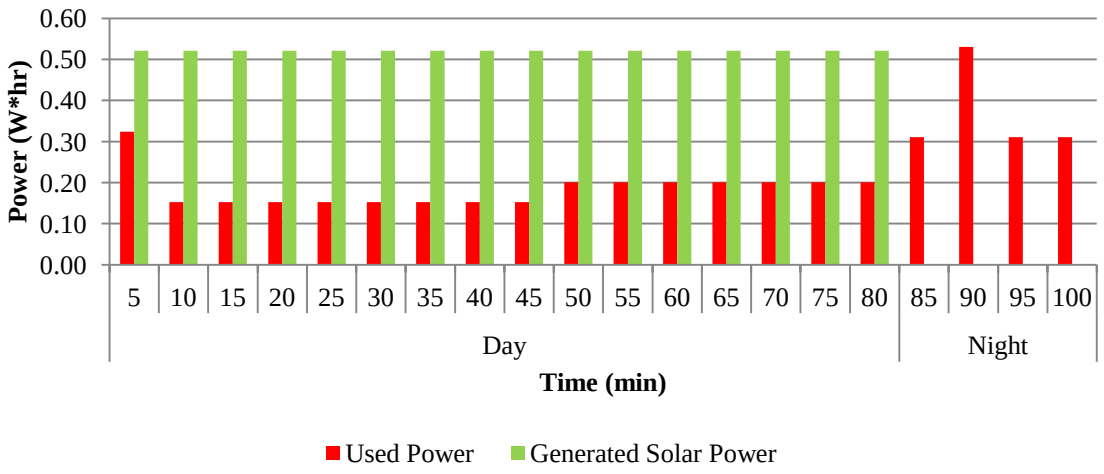

Figure 10: Power Balance for One Orbit

As Figure 10 shows, during a typical orbit there is plenty of excess power generated that can be used to charge the battery. During the night period, the battery will then produce the required amount of power to continue the full operation of the satellite.

CHAPTER FOUR: OPTIMAL POWER MANAGEMENT

There are several challenges that must be overcome when it comes to power scheduling for small satellites. (1) The lack of constant communication between the satellite and ground stations means that the operators must preload a schedule of events for the satellite to accomplish between ground accesses. If an unforeseen circumstance occurs that affects the power usage of the craft, the predefined power schedule might no longer be accurate. Additionally, it may not even be possible to accomplish the scheduled events due to a lack of power availability. (2) Operators that are responsible for monitoring the status of the spacecraft must be on call 24 hours-a-day, 7 days-a-week[19]. These teams of operators can become quite large, even for small satellites. For example, nine full-time staff members were required to monitor and operate the Los Alamos National Laboratory's ALEXIS satellite[20]. (3) Operational costs for satellites can make up a large portion of the total mission cost. Several studies have shown that operations can range between 5 - 40% of the total mission cost[21,22,23].

Therefore, it would be useful to have a way that the satellite could schedule its own power usage, and also respond to any abrupt changes in the status of the satellite such as damage, solar panel failure, battery outages, or, in our case, a dust strike that occurs at a time that cannot be predicted. Adding an autonomous power scheduling system can also reduce operating personnel demands and operating costs[24,25]. In order to properly schedule different events, inspiration has been taken from power grid management algorithms that have been developed for self-contained, off-grid systems such as the so called "smart" homes and communities or power systems from hybrid vehicles[26,27,28].

Power Usage Modeling

The power usage of each subsystem is modeled following the general form outlined in[29]. The majority of the subsystem dynamic equations are of the on/off type of system. These equations, encompassing the power usages of the payload, C&DH, and thermal subsystems, are modeled as

$$x_{dust}(t+1) = P_{dust}u_{dust}(t), \qquad u_{dust}(t) \in U = \{0,1\} \qquad (5)$$

$$x_{thermal}(t+1) = P_{therm}u_{therm}(t), \qquad u_{therm}(t) \in U = \{0,1\} \qquad (6)$$

$$x_{CPU}(t+1) = \sum_{i=0}^{N} u_{CPU,i}(t)P_i, \qquad u_{CPU,i}(t) \in U = \{0,1\} \qquad (7)$$

where P_{dust}, P_{therm}, and P_i are the power consumptions of the dust detector, thermal subsystem, and each CPU process (such as analog-to-digital conversion, serial communication, or micro SD storage/retrieval), respectively. The various u values are the inputs to these subsystems. Here, a u value of 0 equates to 'off', whereas a u value of 1 represents 'on'. Also, the input to the CPU is a group of 1s and 0s corresponding to whether a particular internal process needs to be active or not. It should be noted that the CPU has a minimum resting power requirement, and as such, could be treated differently than a simple on/off system. However, with the compartmentalized nature of the CPU, the sleep mode state can be considered as having only the sleep mode process

'on' and all the other processes 'off'. Thus it can be treated as part of the on/off family described previously.

For the other major subsystems, a combination of the on/off structure and an "always on" structure is used. Though systems that are always on cannot be scheduled, there is still variability in the amount of power that is drawn by them. This problem is solved by treating them as an on/off system with a variable and constant term, where the lower bound is the minimum required power, as opposed to a value of zero. That way, when the system is 'off' it will be requesting no power for the transmitter, but is still resting at some minimum required power level. This form is shown below for the communication subsystem

$$x_{comm}(t+1) = P_{rec_{sat}} + P_{trans_{sat}}(t), \qquad P_{trans_{sat}}(t) \in U = \{0, \ldots, P_{trans_{\max}}\} \qquad (8)$$

where $P_{rec_{sat}}$ is the power required by the receiver and $P_{trans_{sat}}$ is the power required by the transmitter. $P_{rec_{sat}}$ is a constant value, and $P_{trans_{sat}}$ is modeled by the Friis Transmission Equation[30] as

$$P_{trans_{sat}} = \frac{16\pi^2 R^2 P_{rec_{ground}}}{G_{trans_{sat}} G_{rec_{ground}} \lambda^2} \qquad (9)$$

where R is the distance between the antennas, $P_{rec_{ground}}$ is the input power of the ground station receiving antenna, $G_{trans_{sat}}$ is the gain of the satellite transmitter, $G_{rec_{ground}}$ is the gain of the ground

station receiving antenna, and λ is the wavelength. This transmission power is determined as a part of the satellite's link budget. We require the link budget to have a margin of at least 10 dB. However, the actual margin is flexible, and as long as it is above the 10 dB limit, the transmission power corresponding to the margin can change. If the power requested by the communication subsystem violates the maximum power constraint, the scheduler will first try to reduce the power that needs to be sent to the transmitter. If the power cannot be reduced further without violating the link budget margin constraint, the scheduler will then shift the desired communication time.

Similar to the communication subsystem, the equation for the power required by the ADC subsystem is shown below,

$$x_{ADCS}(t+1) = P_{ADCS_{\min}} + P_{ADCS_{req}}(t), \qquad P_{ADCS_{req}}(t) \in U = \{0,\ldots,P_{ADCS_{\max}} - P_{ADCS_{\min}}\} \quad (10)$$

where $P_{ADCS_{\min}}$, $P_{ADCS_{\max}}$, and $P_{ADCS_{req}}$ are the minimum, maximum and requested power for the ADCS. The specific value requested by the ADCS will come from an offline computation that uses the current orbital and attitude information to determine the optimal amount of torque it will take to make a maneuver, along with the power needed to accomplish that maneuver.

Finally, the battery (shown below) is modeled as a charging/discharging system.

$$x_{batt}(t+1) = \begin{cases} \min\left(x_{batt}(t) - r_d V_d + r_c V_c, P_{batt_{\max}}\right) & if\ u_{batt} = 1 \\ \max\left(x_{batt}(t) - r_d V_d, 0\right) & if\ u_{batt} = -1, \quad u_{batt}(t) \in U = \{-1,0,1\} \\ x_{batt}(t) & if\ u_{batt} = 0 \end{cases} \quad (11)$$

Here, $u_{batt} = -1$ is when the battery is in a discharging state, $u_{batt} = 0$ is a holding state, and $u_{batt} = 1$ is a charging state. Additionally, r_c is the charge rate of the battery in Amps, V_c is the charging voltage supplied to the battery, r_d is the discharge rate of the battery in Amps, V_d is the discharge voltage supplied by the battery, and $P_{batt_{\max}}$ is the maximum amount of power that can be stored in the battery. It is important to closely monitor the state of the battery for several reasons. (1) The battery is not always a generating unit, thus its place in the power balance equation changes: (2) The battery is not a limitless source of power like the solar panels (in terms of capacity not time of usage) that can be used indefinitely: (3) The depth of discharge of the battery is an important quantity that is closely related to the longevity and long term efficiency of the battery. Thus, the state of the battery must be closely monitored even though, as will be shown, the state does not directly affect the battery term in the power balance equation.

The current orbital state of the satellite will play a large role in the state of the battery. In addition to determining whether it is even possible to charge the batteries, the orbit will affect how much power is being generated by the solar panels, which, combined with information about the current demands on the power supply, will control how much power can be allocated to battery charging. The solar panels will be the main source of power during the day time and will route power through the batteries to the subsystems while simultaneously charging the batteries with the surplus power. Therefore, the batteries will be in a charging and discharging state at the same time when the craft is not in eclipse. During eclipse periods, the batteries will be the main source of power and will be represented as solely discharging. Thus, in light of the

dynamic nature of the battery system, it has a more complicated set of equations to better represent the state of the battery and how it affects the power balance of the satellite.

Cost Function

While the dynamics of the subsystems deal solely with requested power, the cost function of the algorithm considers the schedule of events. The performance index is formatted as follows,

$$J = min \sum_{i=1}^{n} \sum_{j=t_0}^{t_f} W_i \left| u_{current_{i,j}} - u_{schedule_{i,j}} \right| \quad (12)$$

$$s.t. \quad P_{req_i} \leq P_{supply_i} \quad (13)$$

$$x_{batt}(t) > DoD * P_{batt_{\max}} \quad (14)$$

where n is the number of subsystems needing to be scheduled, t_0 is the initial scheduled time, t_f is the final scheduled time, W is an arbitrary weight assigned to each subsystem that represents the flexibility of the subsystem to deviation from its desired schedule, and $u_{current_{i,j}} - u_{schedule_{i,j}}$ is the difference between the desired/scheduled operation time and any changes to the schedule that need to be made to accommodate the power balance. The systems ordered from most flexible to least flexible are as follows: ADCS, Communications, Thermal, Dust Detector, and CPU. The desired schedule will be predetermined and will represent the

typical distribution of power during an orbit. The satellite will deviate from it as necessary but will reset to the desired value if possible.

The power balance mentioned earlier is represented by Equation 13, where P_{supply_i} is the maximum amount of power that can be supplied at any given time by the battery, and P_{req_i} is represented by,

$$P_{req_i} = x_{dust_i} + x_{therm_i} + x_{CPU_i} + x_{comm_i} + x_{ADCS_i} \quad (15)$$

This power balance is the major constraint on the cost function. All of the power being used by the satellite at any given time must be less than the maximum amount of power the satellite is able to provide. In this way, the power requirement derived from the dynamics is related to the cost function, which only deals with the schedule. The goal of the cost function is to force the satellite to adhere to its scheduled power outputs as much as possible. Thus, the ideal, minimal performance index is actually the desired schedule. If the desired schedule violates the power balance constraint, the weights on the subsystems become active. Additionally, the cost increases as the solution moves farther from the desired schedule, ensuring that the solver adheres to the desired schedule as closely as possible. The second constraint on the system is that the battery must stay above some arbitrary charge level. This level is mission flexible, but we set the value to a depth of discharge (DoD) of 30% of the maximum storage capability.

Preliminary Results

Using the linear programming solver in Matlab to solve the scenarios resulted in the simulations shown below. The first scenario tested the response of the scheduler to an unexpected event, namely a dust strike. The Figure 11 shows the normal operation schedule, with only the thermal subsystem being active during the eclipse period at the end of the orbit, and a maximum power of 6.25 W. Figure 12 shows a series of events triggered by a dust strike. The dust strike causes the CPU to respond and record the data, after which the ADCS is activated to correct any perturbations caused by the strike. Finally, a communication with the ground station is scheduled. All of the following events are well within the maximum power limit, so no other management or optimization is required.

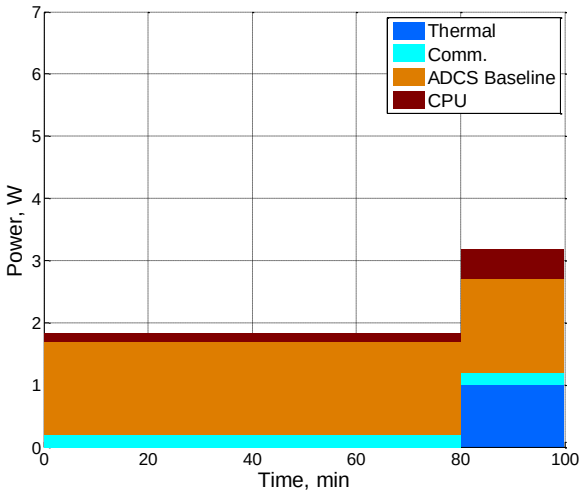

Figure 11: Power Schedule Prior to Dust Strike

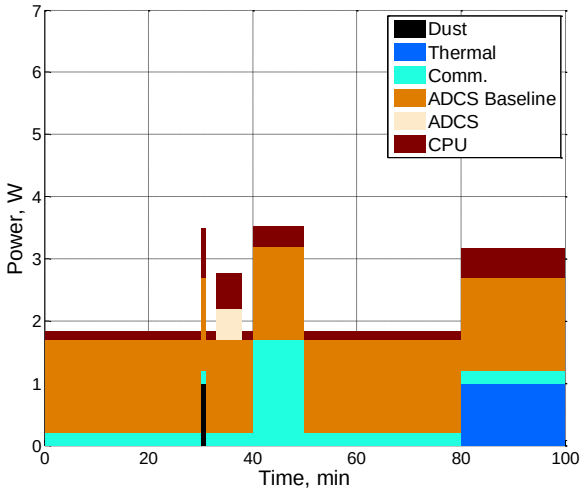

Figure 12: Power Schedule Post Dust Strike

In order to demonstrate a situation where rescheduling is required, the following scenario is introduced in Figures 13-15. Note that the "nighttime" is shown in the middle of the orbital period rather than at the end. A dust strike interrupts a regularly scheduled, nighttime communication with a ground station, shown in Figure 13. Several batteries have failed, and as such, there is only 4.5 W available. The dust strike activates the response from the ADCS and the ground communication sequence. However, as is shown in Figure 14, the loss of power prevents all of these activities from being performed concurrently as they violate the reduced power constraint. The scheduler is able to take the new available power, update the constraints, and recalculate a schedule that allows for a resumption of the communication with the ground after the dust strike data is recorded. This is followed by a maneuver to correct for any attitude changes caused by the strike. The optimization is shown in Figure 15. Additionally, the scheduler attempted to reduce the amount of power sent to the transmitter in an effort to avoid interrupting the communication in progress. Since it was not able to reduce the power in such as

way that did not violate the link margin constraint, it stopped transmitting while the strike occurred, and resumed transmission once power was available. These results tentatively indicate the success of the scheduler. Greater flexibility for the solver, along with a more extensive range of tests is currently in progress.

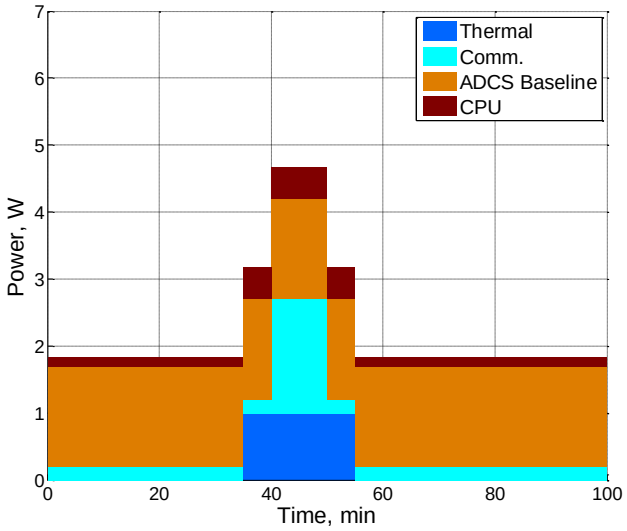

Figure 13: Power Schedule Prior to Dust Strike

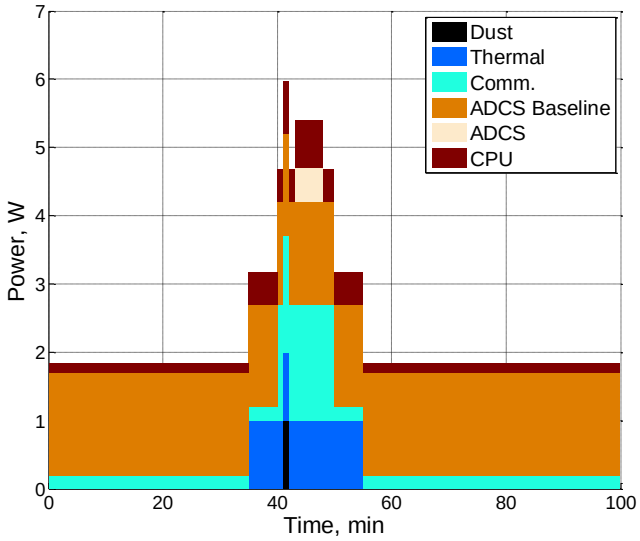

Figure 14: First Reschedule Attempt

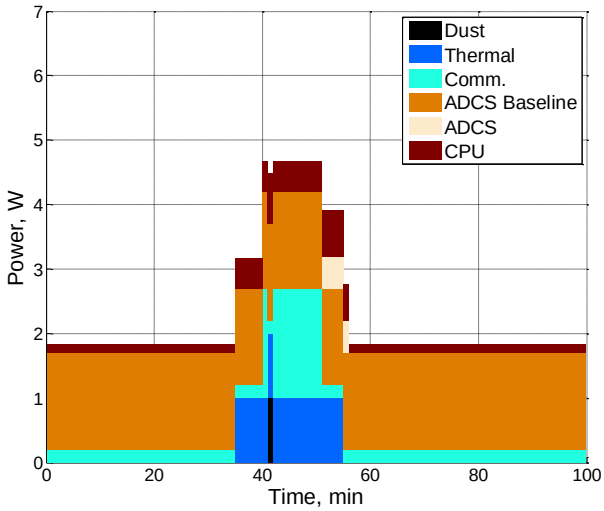

Figure 15: Final Optimized Schedule

CHAPTER FIVE: CONCLUSIONS AND FUTURE WORK

A possible dust detector mission is designed for a pico-scale satellite in a low earth orbit. Preliminary hardware for the mission is chosen and preliminary mass and power budgets are analyzed. Along with a new attitude guidance method, an innovative power scheduling algorithm is detailed and an initial set of results are obtained. Through this analysis, the feasibility of the mission has been demonstrated.

This mission has many benefits, including increasing the available information about the composition of the space environment near Earth, and aiding in the design of dust particle impact mitigation systems on future satellites. In addition to these benefits, the new power scheduler developed for this mission can be useful for keeping a satellite operational should there be an unexpected event when contact with the ground is not available. This power management strategy can be applied to larger satellites or robotic missions.

Future work on this topic includes adapting more accurate power usage, generation and storage models into a nonlinear format and using a nonlinear solver. In addition to refining the solver, enhancements to the other subsystem models are planned. These power models are almost entirely theoretical, and as such, can be validated through testing of the hardware that is planned for use in the satellite.

LIST OF REFERENCES

[1] Lee, S., Hutputanasin, A., Toorian, A., Lan, W. and R. Munakata, "CubeSat Design Specification (Rev 12)," The CubeSat Program, California Polytechnic State University, 2009. http://www.cubesat.org, [Cited 11 Apr. 2012].

[2] Lan, W. "Poly Picosatellite Orbital Deployer Mk III ICD (Rev 0)" The CubeSat Program, California Polytechnic State University, 2007, URL: http://www.cubesat.org/ [cited 11 April 2012].

[3] Burlacu, M., and P. Lorenz, "A Survey of Small Satellites Domain: Challenges, Applications and Communications Key Issues," ICaST Magazine, ICST, Sept. 24, 2010, URL: http://icast.icst.org/2010/09/survey-small-satellites-domain-challenges-applications-and-communications-key-issues [cited 16 April 2012].

[4] Berezhnoy, A. A., "Meteoroid bombardment as a source of the lunar exosphere," Advances in Space Research, vol. 45, No. 1, 2010, pp. 70-76.

[5] Borin, P., Cremonese, G., Marzari, F., Bruno, M., and S. Marchi, "Statistical analysis of micrometeoroids flux on Mercury," Astronomy & Astrophysics, vol. 503, 2009, pp. 259-264.

[6] Horanyi, M., Hoxie, V., James, D., Poppe, A., Bryant, C., Grogan, B., Lamprecht, B., Mack, J., Bagenal, F., Batiste, S., Bunch, N., Chanthawanich, T., Christensen, F., Colgan, M., Dunn, T., Drake, G., Fernandez, A., Finley, T., Holland, T., Jenkins, A, Krauss, C., Krauss, E., Kauss, O., Lankton, M., Mitchell, C., Neeland, M., Reese, T., Rash, K., Tate,

G., Vaudrin, C., and J. Westfall, "The Student Dust Counter on the New Horizons Mission," Space Science Reviews, vol. 140, No. 104, 2006, pp. 387-402.

[7] Poppe, A., James, D., and M. Horanyi, "Measurements of the terrestrial dust flux variability by the Cosmic Dust Experiment," Planetary and Space Science, vol. 59, 2011, pp. 319-326.

[8] Simpson, J. A., and A. J. Tuzzolino,, Nuclear Instruments and Methods, A236, 1985, pp. 187–202.

[9] CubeSatShop.com, "Cube Computer," Electronic Systems Laboratory, URL: http://www.isispace.nl/brochures/CubeComputer%20Brochure_CSS.pdf, [cited 31 January 2013].

[10] CubeSatShop.com, "VHF downlink UHF uplink full-duplex transceiver," ISIS, URL: http://www.cubesatshop.com/index.php?page=shop.product_details&product_id=73&flypage=flypage.tpl&pop=0&option=com_virtuemart&Itemid=65, [cited 31 Jan. 2013].

[11] Radio Regulations Articles Edition of 2008 Article 22 Section 1 (RR 22.1 § 1), International Telecommunications Union – Cessation of Emissions.

[12] CubeSatShop.com, "Deployable Antenna for CubeSats," ISIS, URL: http://www.cubesatshop.com/index.php?page=shop.product_details&flypage=flypage.tpl&product_id=66&category_id=6&option=com_virtuemart&Itemid=70, [cited 31 Jan. 2013].

[13] Brown, C.D., Elements of Spacecraft Design, AIAA Education Series, Reston, VA, 2002, pp. 396-398.

[14] CubeSatShop.com, “MAI-100 ADCS,” Maryland Aerospace, Inc., URL: http://cubesatshop.com/index.php?page=shop.product_details&flypage=flypage.tpl&product_id=52&category_id=7&option=com_virtuemart&Itemid=69, [cited 15 Apr. 2013].

[15] Develle, M., and Y. Xu, “Optimal Attitude Control Management via the B-Spline Augmented Virtual Motion Camouflage Method,” IEEE Transaction on Aerospace and Electronic Systems, revision submitted.

[16] Cao, C., and N. Hovakimyan, “Design and Analysis of a Novel L1 Adaptive Control Architecture with Guaranteed Transient Performance,” IEEE Transactions on Automatic Control, Vol. 53, No. 2, 2008, pp. 586–591.

[17] Clyde-Space.com, “Small Satellite Solar Panels” Clyde Space Ltd. URL: http://www.clyde-space.com/products/solar_panels, [cited 17 Apr. 2013].

[18] Clyde-Space.com, “CubeSat Standalone Battery” Clyde Space Ltd., URL: http://www.clyde-space.com/cubesat_shop/batteries/16_cubesat-standalone-battery, [cited 17 Apr. 2013].

[19] Shriver, P.M., Palo, S.E., Zenick, R. G., and M. J. Balas, “Reward-Lifetime Scheduling Approach to the Autonomous Spacecraft Power Management Problem,” Journal of Aerospace Computing, Information, and Communication, Vol. 9, No. 2, Sept. 2012, pp. 58-67.

[20] Roussel-Dupré, D., Bloch, J. J., Ciskowski, D., Dingler, R., Little, C., Kennison, M., Priedhorsky, W. C., Ryan, S., and R. Warner, “On-Orbit Science in a Small Package: Managing the ALEXIS Satellite and Experiments,” Proceedings of the SPIE, Advanced

Microdevices and Space Science Sensors, Vol. 2267, Bellingham, Washington, 1994, pp. 76-89.

[21] Wertz, J. R., and W. J. Larson, "Reducing Space Mission Cost," Microcosm Press, El Segundo, CA, 1996.

[22] Sarsfield, L., "The Cosmos on a Shoestring: Small Spacecraft for Space Earth Science," RAND Critical Technologies Inst. Santa Monica, CA, 1998, p. 105.

[23] Harrison S. A., Price, M. E., and M. S. Philpott, "Task Scheduling for Satellite Based Imagery," Proceeding of the 5th International Symposium on Artificial Intelligence, Robotics and Automation in Space, European Space Agency Publications Division, Noordwijk, The Netherlands, 1999, pp. 291-296.

[24] Bernard, D. E., Dorais, G. A., Fry, C., Gamble, E. B., Jr., Kanefsky, B., Kurien, J., et al., "Design of the Remote Agent Experiment for Spacecraft Autonomy," Proceedings of the IEEE Aerospace Conference, IEEE Publications, Piscataway, NJ, 1998.

[25] Singer, J., "Automated Ground System Allows Air Force to Reallocate Personnel," Space News, March, 2008.

[26] Zhang, D., Papageorgiou, L. G., Samsatli, N. J., and N. Shah, "Optimal Scheduling of Smart Homes Energy Consumption with Microgrid" *Energy 2011:* The First International Conference on Smart Grids, Green Communications and IT Energy-aware Technologies, No. c, 2011, pp. 70–75.

[27] Chan, C. C., "The State of the Art of Electric, Hybrid, and Fuel Cell Vehicles" Proceedings of the IEEE, vol. 95, No. 4, 2007, pp. 704–718.

[28] Koot, M., Kessels, J., DeJager, B., Heemels, W., VandenBosch, P., and M. Steinbuch, "Energy Management Strategies for Vehicular Electric Power Systems" IEEE Transactions on Vehicular Technology, vol. 54, No. 3, 2005, pp. 771–782.

[29] Zelazo, D., Dai, R., and M. Mesbahi, "An Energy Management System for Off-Grid Power Systems," Energy Systems, vol. 3, No. 2, June 2012, pp. 153-179.

[30] Friis, H. T., "A Note on a Simple Transmission Formula," Proceedings of the IRE, vol. 34, 1946, pp. 254-256.